J. Biophotonics **9**, No. 3, 218–223 (2016) / **DOI** 10.1002/jbio.201500280

Journal of BIOPHOTONICS

LETTER

Human IgG detection in serum on polymer based Mach-Zehnder interferometric biosensors

*Eva Melnik**, [1], *Roman Bruck*[1], *Paul Muellner*[1], *Thomas Schlederer*[2], *Rainer Hainberger*[1], *and Michael Lämmerhofer*[3]

[1] AIT Austrian Institute of Technology GmbH, Health & Environment Department, Molecular Diagnostics, 1220 Vienna, Austria; homepage: www.ait.ac.at
[2] Phadia Austria GmbH, Part of Thermo Fisher Scientific Immuno Diagnostics, 1220 Vienna, Austria
[3] University of Tübingen, Institute of Pharmaceutical Sciences, Auf der Morgenstelle 8, Tübingen, Germany

Received 21 October 2015, revised 25 November 2015, accepted 26 November 2015
Published online 12 December 2015

Key words: Mach-Zehnder interferometer, polymer waveguide, biosensor, human IgG, polyimide, human serum, injection molding

We report a new method for detecting human IgG (hIgG) in serum on integrated-optical Mach-Zehnder interferometer biosensors realized in a high index contrast polymer material system. In the linear range of the sensor (5–200 nM) we observed excellent signal recoveries (95–110%) in buffer and serum samples, which indicate the absence of matrix effects. Signal enhancement was reached by using secondary anti-human IgG antibodies, which bind to immobilized target IgGs and allow detecting concentrations down to 100 pM. This polymer based optical sensor is fully compatible with cost-efficient mass production technologies, which makes it an attractive alternative to inorganic optical sensors.

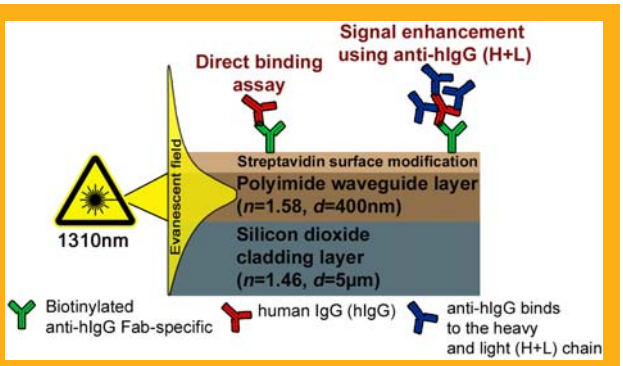

Graphical abstract of the hIgG measured on polymer based photonic sensors using a direct binding assay and a signal enhancement strategy with secondary antibodies.

1. Introduction

The detection of serological biomarkers is important in the daily medical diagnostic routine to evaluate the health, disease or vaccination status [1]. Human immunoglobulin G (hIgG) plays a key role in many medical conditions due to its ability to reflect the status of the immune system. The strong evidence for auto-antigen specific IgG production in autoimmune disorders (e.g. rheumatoid arthritis, Sjögren-Syndrom or Lupus erythematodes) has been recognized as a viable strategy in medical diagnostics [2–4]. Beside diagnosis of autoimmune disorders, analysis of total concentrations of IgG or of pathogen antigen-specific IgGs (viral: e.g. HBV, or bacterial: e.g. helicobacter pylori) [5, 6] is of relevance to support infection diagnosis and monitor the progress of therapy [7]. Common hIgG immunoassays use mi-

* Corresponding author: e-mail: eva.melnik@ait.ac.at, Phone: +43 50550 4309, Fax: +43 50550 4399

crotiter plate or microarray formats, which need time consuming sample preparation steps and complex readout-systems. Due to this reason they are not well suited for Point-of-Care testing (POCT). More promising for POCT are lateral flow [8] and lab-on-chip formats with fully integrated sample preparation. These approaches employ colorimetric, fluorescent, or chemoluminescent detection methods, which prohibit a direct quantitative read-out. Therefore, biosensing concepts are demanded that allow quantitative biomarker detection and facilitate electronic data processing in combination with mobile information technologies [9]. In this context, polymer based sensing device concepts are attracting particular attention due to the prospect of low production costs. For their fabrication, conductive polymers for electrochemical sensors (e.g. tosylate doped poly(3,4-ethylenedioxythiophene, PEDOT)) [10], cellulose for paper based sensors [11], or high refractive index polymers such as OrmoCore (Microresist Technology GmbH, Germany) and polyimide for photonic sensors [12–14] have been investigated. Critical factors for polymer based sensors are the stability, non-specific binding and sensitivity in real samples such as blood or serum [14, 15]. In this study, we employ polyimide waveguide based integrated optical Mach-Zehnder interferometers for the detection of hIgG in a serum matrix. In order to obtain different concentration levels of hIgG we mixed a certified human reference serum, which has a given IgG concentration, with IgG/IgA-free chicken serum. We compared measurements in buffer and mixed-serum and evaluated the signal recoveries. To reach lower detection limits we tested different binding assays by using secondary antibodies and nanoparticulate streptavidin-(anti-hIgG)$_4$ bioconjugates.

2. Materials and methods

2.1 Materials

3-Mercaptopropyl trimethoxysilane (MPTMS), bovine serum albumin (BSA), and streptavidin were purchased from Sigma Aldrich, Vienna, Austria. The polyimide Pyralin® PI-2771 was purchased from HD Microsystems, Neu-Isenburg, Germany, and the polymer cladding material Ormoclad from Microresist Technology GmbH, Berlin, Germany. Maleimide-PEG$_2$-biotin (M-PEG$_2$-biotin), 100 mM PBS buffer (pH 7.3) and IgG/IgA free chicken serum (product-nr.: 10-9498-01) were supplied by Thermo Fisher Scientific, Vienna, Austria. The goat anti-human IgG (Fab specific) with long-spaced biotin, the human IgG and the goat anti-human IgG (H + L) with long-spaced biotin were purchased from Jackson ImmunoResearch, Newmarket, United Kingdom.

Table 1 Certified reference values of protein concentrations in the employed certified human serum.

Proteins	Certified value (g/L)	Uncertainty (g/L)
α1-antitrypsin	1.12	± 0.03
albumin	37.2	± 1.2
haptoglobin	0.889	± 0.021
IgA	1.8	± 0.05
IgG	9.17	± 0.18
IgM	0.723	± 0.027
transferrin	2.36	± 0.08

The certified human serum (ERM-DA470k/IFCC HUMAN SERUM) was supplied by the Institute for Reference Materials and Measurements and purchased from Sigma Aldrich, Vienna, Austria. The certified reference values of the relevant protein concentrations in this certified human serum are listed in Table 1.

The maximum concentration of hIgG (M_r = 150 kDa) in the serum was 9.17 ± 0.18 g/L, which corresponds to 61.3 µM. From this known hIG concentration we prepared standards in the concentration range between 0.1–800 nM by diluting the human serum with IgA/IgG-free chicken serum to maintain the matrix effect of real samples.

2.2 Sensor-chip processing

The polyimide based Mach-Zehnder interferometer (PI-MZI) sensors were processed as reported before [16]. The inverted rib waveguide structures were patterned onto 3 × 3 cm^2 pieces of monocrystalline silicon covered with a 5 µM silicon dioxide layer using conventional photolithography and an SF_6 reactive ion etching process. The 2.2 µM wide waveguide structures were etched 150 nM deep and filled in the next step by spin-coating polyimide as waveguide material. The spin-coated films were soft baked at 100 °C (1 min), exposed to UV light at 365 nM (570 mJ/cm^2) and finally hard baked at 200 °C (1 h). In order to protect the reference arm of the MZI sensors, the inorganic–organic hybrid polymer cladding material Ormoclad was spin-coated on the polyimide layer, soft baked at 120 °C (2 min), structured with UV-light at 365 nM by using a chromium-mask (1710 mJ/cm^2), post baked at 120 °C (2 min), washed in developer, and finally hard baked at 150 °C (3 h). The sensors used in this study were processed in three batches on different days and functionalized on the following day.

2.3 Surface functionalization

The sensors were biotinylated and streptavidin coated as described previously [17]. In a first step, the sample surfaces were activated with oxygen plasma (1 min, 40 W power, 1 mbar; 2.45 GHz low pressure plasma system FEMTO, Diener electronic GmbH, Ebhausen, Germany). For silanization, the samples were dipped for 1 h in acidic aqueous MPTMS solution composed of (3% (v/v) MPTMS in 0.07 M acetate buffer pH 5.5, 2.8% (v/v) TritonX-100, and 25% (v/v) methanol). The biotinylation of the surfaces was performed by dipping the samples in binding buffer (50 mM phosphate-buffered saline, PBS, pH 7.0 with 10% (v/v) 2-propanol) for 2 h. The biotinylated MZI-sensors were stored at 4 °C vacuum packed for a maximum time of two weeks.

Before starting with the hIgG measurements, the PI-sensors were modified with streptavidin and the biotinylated anti-human IgG (Fab specific). These processes were monitored on the polyimide-MZI sensors, in order to evaluate the reproducibility of the biofunctionalization.

2.4 Photonic measurement setup

The polyimide based Mach-Zehnder interferometric sensors were used for photonic biosensing. A tuneable laser with a central wavelength of 1310 nm acted as light source. The in- and out-coupling of light to and from the optical waveguide was performed by end-face coupling from optical fibers. In the MZI sensor, the light propagating in the input waveguide is split into the sensing and the reference arm and recombined after 10 mm distance by means of Y-junctions (see Figure 1). The reference arm is covered with the cladding material Ormoclad, which ensures that only the target molecule binding to the sensing waveguide lead to a sensor response. Due to these target-analyte binding events, a local change in the refractive index occurs, which influences the propagation of the light guided in the sensing arm. This leads to a sinusoidal modulation of the output signal at the end of the interferometer as function of the effective index of the measurement arm. The relationship between the normalized output power P_{out}/P_{in}, and the difference of the effective indices Δn_{eff} between the sensing and the reference arm is given by

$$\frac{P_{out}}{P_{in}} = \frac{1}{2}[1 + \cos(\Delta n_{eff} L k_0)] \quad (1)$$

wherein L is the measurement window length and k_0 the wavenumber in vacuum. From Eq. (1), the accumulated phase shift $\Delta\Phi = \Delta n_{eff} L k_0$ can be calculated, which correlates with the amount of target molecules captured on the surface.

In order to enable the measurement of target proteins in liquids, a polydimethylsiloxane fluidic chamber was mounted on top of the biotinylated sensor. The MZI-sensor measurement setup consisted of a piezo-electric alignment stage for precise fiber-to-waveguide coupling and a fluidic control system with an electronically controlled host-syringe pump system (flow rate: 20 µl/min, minimum sample volume: 100 µl). These components were operated by a single control software (see Supporting information).

3. Results and discussion

Three batches of sensor chips were processed as described above on different days and biotinylated shortly after fabrication. Before starting with the hIgG measurements, the biotinylated PI-MZI sensors were evaluated with respect to their homogenous sensing performance. For this purpose, we monitored the sensor responses to a refractive index change of $\Delta n = 0.0038$ induced by exchanging ultrapure water with PBS buffer. The corresponding signal amounted to a phase shift of $4.10 \pm 0.57\,\pi$ ($n = 15$). Subsequently, the streptavidin immobilization was monitored at flow rates of 20 µl/min in PBS buffer with a protein concentration of 50 µg/ml. The observed phase shift was $2.87 \pm 0.67\,\pi$ ($n = 14$). Next, biotinylated anti-human IgG (Fab-specific) was immobilized on the streptavidin layer (100 µg/ml biotinylated antibody in PBS buffer), which gave an additional phase shift of $2.52 \pm 0.67\,\pi$ ($n = 13$). In a first step, the label-free hIgG measurements were performed with a direct binding assay in buffer and mixed-serum samples. The hIgG concentrations ranged from 5 nM to 200 nM (see Figure 1). Since both

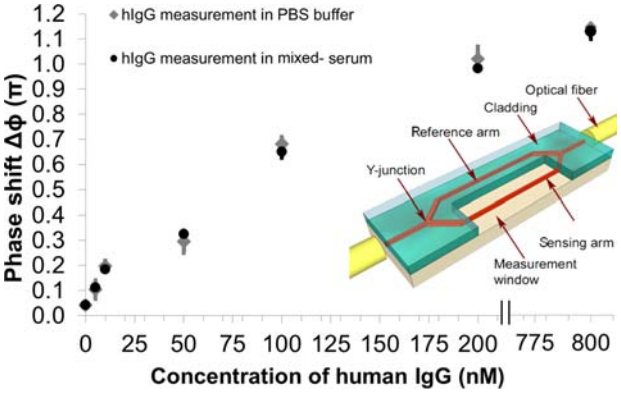

Figure 1 Comparison of hIgG measurements in PBS buffer and mixed-serum samples.

calibration curves exhibit the same slope, and excellent signal recoveries (95–110%) were observed, these results prove that serum matrix effects (e.g. competitive binding events, non-specific binding) are negligible for our system and do not impact the performance of the functionalized polyimide waveguide layer. The limit of detection (LOD) was calculated using the definition of LOD = $y_{\Delta\varphi} + 3x\sigma$, where $y_{\Delta\varphi}$ is the average value and σ the standard deviation of the blank measurements (no hIgG present). The blank measurements were performed in buffer ($\Delta\varphi \sim 0.04 \pm 0.015\,\pi$; $n = 4$) and in chicken serum ($\Delta\varphi \sim 0.043 \pm 0.01\,\pi$; $n = 4$). From these values an LOD of 3.2 nM was calculated for hIgG.

In order to pursue a lower detection limit, we evaluated two different label based signal enhancement strategies with secondary antibodies supported binding assays for increased interaction with the evanescent field. From the three layer equation of dielectric waveguides [18] it follows that the penetration depth of the evanescent field into the measurement media is about 100 nM for our polymer based MZI-sensors.

As first signal enhancement approach (see Figure 2A), we used a secondary anti-hIgG antibody that attaches to the heavy and the light chain (H + L) of the target hIgG. The secondary antibodies have broader epitope recognition behaviour than fragment specific antibodies. This recognition behaviour leads to multiple bindings of the secondary antibodies to the immobilized hIgG, which induces higher signals than the single binding event of the hIgG. As a second signal enhancement approach (see Figure 2B) we employed nanoparticulate streptavidin-(anti-hIgG)$_4$ bioconjugates that feature a huge hydrodynamic diameter of about 35 nM (streptavidin ~5 nM, anti-hIgG (H + L) ~15 nM). The binding of these nanoparticulate bioconjugates to the immobilized target hIgG was therefore expected to lead to a significantly higher signal in comparison to the direct binding event of the hIgG under saturation conditions. In order to compare these two label based signal enhancement approaches, we immobilized the hIgG at a saturating concentration of 800 nM on the functionalized sensor surface. Subsequently, we monitored the signal of the streptavidin-(anti-hIgG)$_4$ bioconjugate and the secondary anti-hIgG (H+L), which amounted to $\Delta\varphi \sim 5.17 \pm 0.5\,\pi$ ($n = 4$) and $\Delta\varphi \sim 4.65 \pm 0.44\,\pi$ ($n = 4$), respectively (each 50 µg/ml).

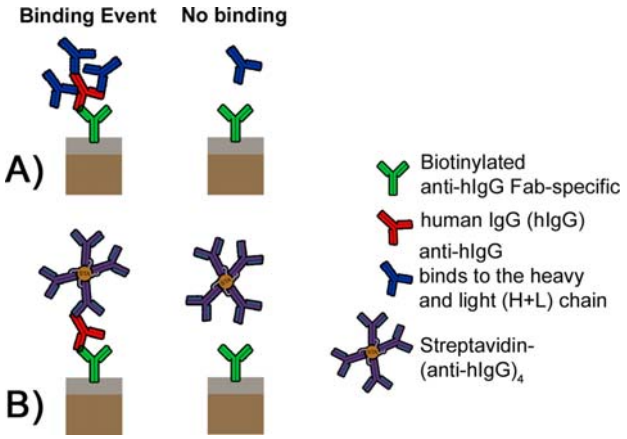

Figure 2 Signal enhancement strategies tested in this study: (**A**) anti-hIgG that binds to different epitopes on the heavy and light chain (H + L) of the immobilized target hIgG; (**B**) nanoparticulate streptavidin-(anti-hIgG)$_4$ bioconjugate.

For a better understanding of these results, we monitored the non-specific binding (see Figure 2) of the streptavidin-(anti-hIgG)$_4$ biomolecules and the secondary anti-hIgG to the streptavidin surfaces with immobilized receptor anti-bodies (i.e. no target hIgG was immobilized). The strept-avidin-(anti-hIgG)$_4$ bioconjugate showed a significant non-specific binding to the surface ($\Delta\varphi \sim 0.5 \pm 0.012\,\pi$ ($n = 14$)), while non-specific binding of the secondary anti-hIgG (H + L) was negligible ($\Delta\varphi \sim 0.023 \pm 0.017\,\pi$ ($n = 4$)). Based on these results, we limited the subsequent experiments to the signal enhancement approach employing secondary anti-hIgG (H + L). Measurements were performed for different hIgG concentrations down to 0.1 nM (see Figure 3). The signal behaviour over the full measurement range (0.1–800 nM) indicates the existence of two binding sites with different binding kinetics. This two-site saturation behaviour can be described by the Langmuir equation (see supporting information). However, in this study we focussed on signal enhancement strategies for lower concentration ranges, in which the secondary binding sites do not play a significant role. The saturation of the primary binding sites with secondary antibodies occurs at about 50 nM hIgG (see Figure 3). The dynamic linear response behaviour shifted to lower concentration ranges and enabled the measurement of 0.1 nM (15 ng/ml) hIgG. The LOD of this signal-amplified

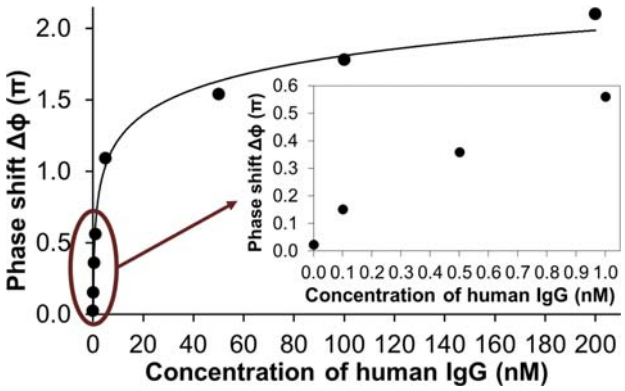

Figure 3 Measurement of hIgG by using the enhancement strategy with the secondary anti-hIgG (H + L).

Tabelle 2 Medical applications of hIgG measurement and typical concentrations.

Application	Diagnostic example	hIgG in serum (nM)	Literature
Health status	Healthy control	79 266	[20]
Diagnostic	Rheumatoid arthritis	16 898	[21]
Diagnostic	Helicobacter pylori	1 430	[22]
Vaccination Status	Hepatitis A*	19.1	[23]
Vaccination Status	Hepatitis B*	2.4	[24]

* the amount of hIgG in nM is calculated from the literature values [19] and from the WHO information found in the description of the "Second International Standard for anti-hepatitis B surface antigen" Nr.: Version 1.0, Dated 22/10/2008).

assay is 0.03 nM (4.5 ng/ml), which is tantamount to an increase in sensitivity of a factor 100, in comparison to the direct binding assay (LOD = 3.4 nM).

With direct binding assay and signal-amplified assay with secondary detection antibodies a concentration range between 0.1–200 nM was covered, which is adequate for various diagnostic applications. Table 2 gives a few examples of required detection limits for medical applications such as the confirmation of the hepatitis B (required lower limit 2.4 nM) or hepatitis A vaccination status (lower limit 19.1 nM) [23, 24]. For the analysis of samples from rheumatoid arthritis patients (~17 000 nM), sample dilutions by a factor of at least 100 will be necessary in order to be in the linear range of the current bioassays [21].

Reports on photonic biosensing in literature are dominated by fully inorganic device concepts, for which many examples of different biomarker measurements in buffer and serum have been published [27]. Inorganic material systems are popular choices as one can rely on well-established semiconductor fabrication technologies for sample processing. Additionally, according to the theory of evanescent sensing, inorganic sensors exhibit a higher sensitivity than polymer based sensors due to the higher achievable refractive index contrast of the waveguide layer to the surrounding medium [14]. Nevertheless, because of the prospect of lower production costs, the development of all-polymer based photonic sensing devices has been attracting increasing interest [12, 13, 25]. So far, only a few examples for molecular sensing can be found in literature and these are limited to buffer solutions [26].

Detection of hIgG on photonic biosensors has so far been only reported for fully inorganic sensor devices. For example, Schmitt et al. measured hIgG in buffer solution on a Young Interferometer at concentrations down to 0.27 nM [28], and Ramachandran et al. detected hIgG on a microring resonator down to a concentration of 0.17 nM [29] (see Table 3).

In both studies, a direct binding assay was used for the detection of the human IgG. Recently, Platte et al. detected human IgE on a dual polarisation interferometry based platform by using a nanoparticle label based binding assay. This assay allowed detecting hIgE in serum samples down to 0.38 nM with a detection limit of 4 pM [30]. Table 3 compares these results with the performance of our polymer waveguide based biosensor.

4. Conclusion

In this study, we performed human IgG measurements in a serum matrix on polymer based optical waveguide sensors. With the label-free binding assay, where the hIgG binds directly to the immobilized receptor molecules, concentrations in the range of 5–200 nM were measured and a LOD of 3.1 nM was achieved in a complex serum environment. The direct binding assay and control measurement results proved the absence of serum matrix effects.

The use of a secondary anti-hIgG antibody (H + L) allowed detecting concentrations down to 100 pM with an LOD of 30 pM. This LOD is suitable for different medical diagnostic applications such as the detection of the Hepatitis A/B vaccination status in serum. In comparison with other inorganic based photonic sensor concepts we can conclude that the polymer based sensor has, in combination with the label based binding assay, comparable LODs and dy-

Table 3 Comparison of IgG detection performance.

Sensor	Detection limit (nM)	Measurement Range (nM)	Literature
Young Interferometer*	0.270	0.270–300	[28]
Optical Micro-ring resonators*	0.17	0.17–2.73	[29]
Dual Polarisation Interferometry*	0.004	0.38–390	[30]
Present Work on Polyimide based sensor	0.03	0.1–200	

* Fully inorganic device concepts

namic ranges. This makes the polymer-based optical sensor a potentially much more cost-effective alternative to inorganic optical sensors concepts.

Supporting Information

Additional supporting information may be found in the online version of this article at the publisher's website.

Acknowledgements This work was supported by the Austrian NANO Initiative under the grant PolyIMPD (project no. 836094).

References

[1] M. Polanski and N. L. Anderson, Biomark. Insight. **1**, 1–48 (2007).
[2] K. Conrad, D. Roggenbuck, D. Reinhold, and T. Dörner, Autoimm. Rev. **9**(6), 431–435 (2010).
[3] J. M. Nielen, Ann. Rheum. Dis. **64**(8), 1199–1204 (2005).
[4] C. Eriksson, H. Kokkonen, M. Johansson, G. Hallmans, G. Wadell, and S. Rantapää-Dahlqvist, Arthritis. Res. Ther. **13**(1), R30 (2011).
[5] S. J. Challacombe, R. S. Percival, and P. D. Marsh, Oral Microbiol. Immunol. **10**(4), 202–207 (1995).
[6] L. A. Amado, L. M. Villar, V. S. de Paula, A. J. de Almeida, and A. M. C. Gaspar, Mem. Inst. Oswaldo Cruz **101**(2), 149–155 (2006).
[7] H. Ipp, A. E. Zemlin, R. H. Glashoff, J. Wyk, N. Vanker, T. Reid, and L.-G. Bekker, J. Clin. Immunol. **33** (3), 605–612 (2013).
[8] C. K. Murray, R. A. Gasser, A. J. Magill, and R. S. Miller, Clin. Microbiol. Rev. **21**(1), 97–110 (2008).
[9] S. Wang, F. Inci, G. de Libero, A. Singhal, and U. Demirci, Biotechnol. Adv. **31**(4), 438–449 (2013).
[10] J. Daprà, L. H. Lauridsen, A. T. Nielsen, and N. Rozlosnik, Biosens. Bioelectron. **43**, 315–320 (2013).
[11] Y. Zhu, X. Xu, N. D. Brault, A. J. Keefe, X. Han, Y. Deng, J. Xu, Q. Yu, and S. Jiang, Anal. Chem. **86**(6), 2871–2875 (2014).
[12] R. Kirchner, A. Finn, R. Landgraf, L. Nueske, L. Teng, M. Vogler, and W.-J. Fischer, J. Lightwave Technol. **32**(9), 1674–1681 (2014).
[13] M. Wang, J. Hiltunen, C. Liedert, S. Pearce, M. Charlton, L. Hakalahti, P. Karioja, and R. Myllylä, Opt. Express **20**(18), 20309 (2012).
[14] R. Hainberger, R. Bruck, P. Muellner, K. Roppert, W. Boxleitner, C. Pacher, and N. Finger, in Proc. SPIE 7386, Photonics North, Quebec, Canada, 2009, 73862Q1-15.
[15] X. Luo and J. J. Davis, Chem. Soc. Rev. **42**(13), 5944–62 (2013).
[16] R. Bruck, E. Melnik, P. Muellner, R. Hainberger, and M. Lämmerhofer, Biosens. Bioelectron. **26**(9), 3832–3837 (2011).
[17] E. Melnik, R. Bruck, R. Hainberger, and M. Lämmerhofer, Anal. Chim. Acta **699**(2), 206–215 (2011).
[18] K. Tiefenthaler and W. Lukosz, J. Opt. Soc. Am. B **6**(2), 209 (1989).
[19] D. S. Rowe, B. Grab, and S. G. Anderson, Bull. Wld. Hlth. Org. **46**, 67–79 (1972).
[20] K. A. Patidar, R. N. Parwani, and S. P. Wanjari, J. Oral. Sci. **53**(1), 97–102 (2011).
[21] L. M. H. da Mota, L. L. dos Santos Neto, R. Burlingame, H. A. Ménard, and I. M. M. Laurindo, Rev. Bras. Reumatol. **50**(4), 375–380 (2010).
[22] O. Hanvivatvong, A. Pongpanich, D. Thong-Ngam, N. Thammacharoenrach, and P. Kullavanijaya, Clin. Diagn. Lab. Immun. **11**(3), 618–620 (2004).
[23] R. A. Heijtink, P. M. Schneeberger, B. Postma, and W. Crombach, Vaccine **20**(23–24), 2899–2905 (2002).
[24] J. J. Ochnio, D. W. Scheifele, M. HO, and L. A. Mitchell, J. Clin. Microbiol. **35**(1), 98–101 (1997).
[25] M. Hiltunen, J. Hiltunen, P. Stenberg, S. Aikio, L. Kurki, P. Vahimaa, and P. Karioja, Opt Express **22**(6), 7229–7237 (2014).
[26] M. Wang, J. Hiltunen, C. Liedert, S. Pearce, M. Charlton, L. Hakalahti, P. Karioja, and R. Myllylä, Optics Express **20**(18), 20309–20317 (2012).
[27] A. L. Washburn and R. C. Bailey, Analyst **136**(2), 227–236 (2011).
[28] K. Schmitt, B. Schirmer, C. Hoffmann, A. Brandenburg, and P. Meyrueis, Biosens. Bioelectron. **22**, 2591–2597 (2007).
[29] A. Ramachandran, S. Wang, J. Clarke, S. J. Ja, D. Goad, L. Wald, E. M. Flood, E. Knobbe, J. V. Hryniewicz, S. T. Chu, D. Gill, W. Chen, O. King, and B. E. Little, Biosens. Bioelectron. **23**(7), 939–944 (2008).
[30] G. W. Platt, F. Damin, M. J. Swann, I. Metton, G. Skorski, M. Cretich, and M. Chiari, Biosens. Bioelectron. **52**, 82–88 (2014).